


Observation of 2D Cherenkov RadiationYuval Adiv^{1,*}, Hao Hu^{2,3,*}, Shai Tsesses^{1,*}, Raphael Dahan¹, Kangpeng Wang^{1,4}, Yaniv Kurman¹, Alexey Gorlach¹, Hongsheng Chen⁵, Xiao Lin⁵, Guy Bartal¹, and Ido Kaminer^{1,†}¹*Andrew and Erna Viterbi Department of Electrical and Computer Engineering, Technion, Israel Institute of Technology, 32000 Haifa, Israel*²*School of Electrical and Electronic Engineering, Nanyang Technological University, Nanyang Avenue, Singapore 639798, Singapore*³*Key Laboratory of Radar Imaging and Microwave Photonics, Ministry of Education, College of Electronic and Information Engineering, Nanjing University of Aeronautics and Astronautics, Nanjing 211106, China*⁴*State Key Laboratory of High Field Laser Physics, Shanghai Institute of Optics and Fine Mechanics (SIOM), Chinese Academy of Sciences (CAS), Shanghai 201800, China*⁵*Interdisciplinary Center for Quantum Information, State Key Laboratory of Modern Optical Instrumentation, ZJU-Hangzhou Global Science and Technology Innovation Center, College of Information Science and Electronic Engineering, Zhejiang University, Hangzhou 310027, China* (Received 15 March 2022; revised 24 August 2022; accepted 7 November 2022; published 6 January 2023)

For over 80 years of research, the conventional description of free-electron radiation phenomena, such as Cherenkov radiation, has remained unchanged: classical three-dimensional electromagnetic waves. Interestingly, in reduced dimensionality, the properties of free-electron radiation are predicted to fundamentally change. Here, we present the first observation of Cherenkov surface waves, wherein free electrons emit narrow-bandwidth photonic quasiparticles propagating in two dimensions. The low dimensionality and narrow bandwidth of the effect enable us to identify quantized emission events through electron energy loss spectroscopy. Our results support the recent theoretical prediction that free electrons do not always emit classical light and can instead become entangled with the photons they emit. The two-dimensional Cherenkov interaction achieves quantum coupling strengths over 2 orders of magnitude larger than ever reported, reaching the single-electron–single-photon interaction regime for the first time with free electrons. Our findings pave the way to previously unexplored phenomena in free-electron quantum optics, facilitating bright, free-electron-based quantum emitters of heralded Fock states.

DOI: [10.1103/PhysRevX.13.011002](https://doi.org/10.1103/PhysRevX.13.011002)Subject Areas: Photonics, Plasmonics,
Quantum Physics**I. INTRODUCTION**

Interactions between free electrons and light are of prime importance for fundamental science, applications, and future technology. Examples include Compton scattering, which is utilized in radiation therapy and spectroscopy [1]; photon-induced near-field electron microscopy (PINEM), which exposes femtosecond physical phenomena at the nanoscale [2–4]; dielectric laser

accelerators, which enable chip-scale particle acceleration schemes [5–7]; and cathodoluminescence, which provides powerful microscopy capabilities and facilitates novel nanophotonic light sources [8–12].

Cherenkov radiation (CR) is a well-known effect in this family of interactions, first discovered in 1934 [13,14] from a charged particle surpassing the phase velocity of light in a medium and emitting an electromagnetic shock wave (often seen as a bluish glow). This discovery was the first instance of a wider concept of spontaneous emission as a result of an extended phase matching between the free electron and the emitted light. This general concept requires the particle velocity to match the phase velocity of light along the particle's propagation direction, defining a characteristic emission angle as a function of the particle velocity, when greater than the phase velocity of light.

Today, the term Cherenkov effect is widely used to describe a variety of phenomena that arise from extended

*These authors contributed equally to this work.

†Corresponding author.

kaminer@technion.ac.il

Published by the American Physical Society under the terms of the Creative Commons Attribution 4.0 International license. Further distribution of this work must maintain attribution to the author(s) and the published article's title, journal citation, and DOI.

phase matching between free charged particles and photons in a myriad of materials. CR-type effects have been proposed and observed in a wealth of artificially engineered materials in which the phase velocity of light can be flexibly tailored [15,16], e.g., photonic crystals [17,18], hyperbolic media [19], gain media [20], and negative-index metamaterials [21–23]. Types of CR were also examined for charged particles traveling in close proximity to a material [24,25]. While research in CR led to a rapid succession of theoretical and experimental discoveries spawning many applications [15,26–30], it is still usually observed as a classical wave phenomenon occurring in 3D geometries.

Interestingly, free-electron–light interactions change dramatically with dimensionality, as was extensively explored theoretically [31–35]. At the heart of any light-matter interaction of a free electron lies the same interaction Hamiltonian, which has the form of a scalar product of the electron momentum and the emitted light field. The scalar product poses a strict limit on the polarization of all electron radiation phenomena—the emitted field must have a polarization component parallel to the electron velocity. Consequently, in 3D, the transverse nature of propagating waves in the optical range constrains the radiation to be emitted sideways (so their polarization can be parallel to the electron momentum). This is why Smith-Purcell-type and CR-type effects in 3D (3D CR) have the radiation emitted

in cones. In contrast, it was predicted that CR into surface waves (2D CR) propagates primarily parallel to the electron trajectory [9,34–39] (Fig. 1), due to the longitudinal nature of these waves in the optical range. This phenomenon bypasses the polarization limit that arises from the interaction Hamiltonian.

The effect of 2D CR was initially predicted in the form of surface plasmon polariton (SPP) modes, also known as Cherenkov-Landau surface shock waves [36,37]. The key to this prediction is the *propagating nature* of SPPs, enabling them to maintain an extended phase matching with the charged particle when it moves parallel to the surface with velocity surpassing the SPP phase velocity. In other cases, SPPs emitted via the extended phase-matched coupling can, in turn, couple out to free space photons and become 3D CR, as predicted in Refs. [38,39]. In any dimensionality, the radiation angle θ (relative to the particle’s trajectory) satisfies $\cos\theta = v_p(\omega)/v_e$, where v_e is the charged particle velocity and $v_p(\omega)$ is the phase velocity of the wave, derived from its dispersion relation and depending on the frequency ω . The dispersion of surface waves causes 2D CR to exhibit an intense narrow spectrum, in sharp contrast to the conventional broadband nature of 3D CR [Fig. 1(e)].

The unique features of 2D CR make it a promising platform to achieve a versatile, tunable, and ultrafast

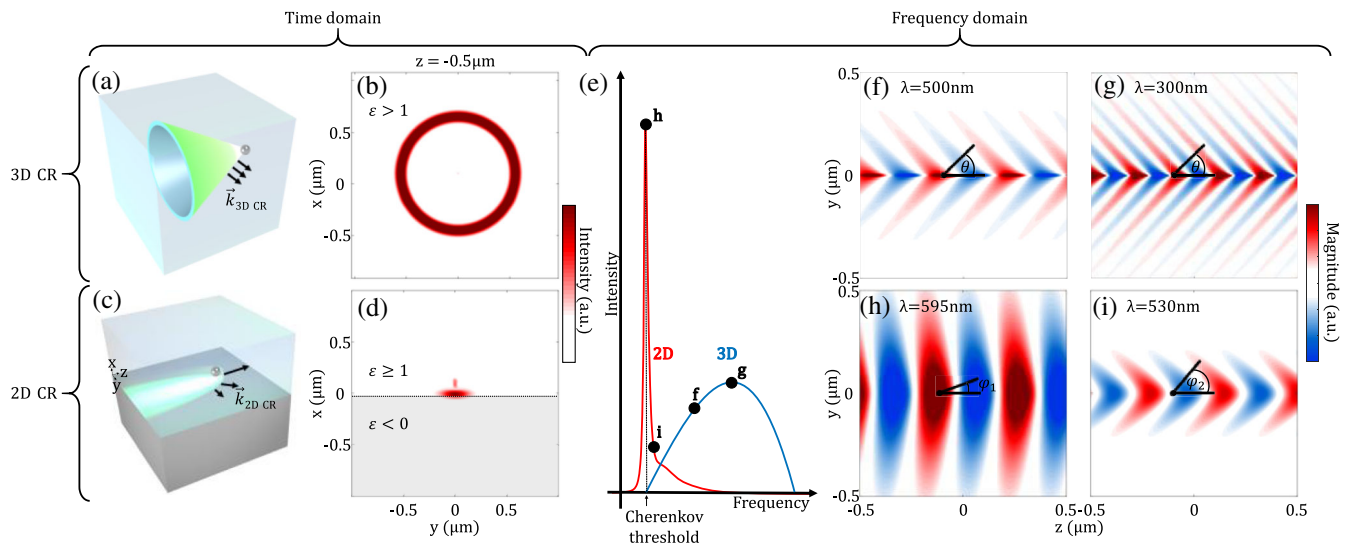


FIG. 1. 3D vs 2D CR: emphasizing their fundamentally different features. (a),(b) Illustration of 3D CR. The radiation is emitted in a set of wave vectors ($\vec{k}_{3D\text{CR}}$) which form a cone (a ring cross section) around the direction of electron velocity, with zero intensity at the direction of motion. (c),(d) Illustration of 2D CR. The radiation is emitted in a set of wave vectors ($\vec{k}_{2D\text{CR}}$) along the 2D surface, with peak intensity at the electron’s direction of motion (shown in the cross section by the peak intensity near the surface). (e) Schematic comparison of 3D CR and 2D CR spectra. Since the dispersion of conventional materials is relatively small and isotropic, the 3D CR spectrum is broad and peaks at a frequency higher than the Cherenkov threshold. In contrast, the 2D CR spectrum is narrow, peaks at the Cherenkov threshold, and decays sharply for large frequencies. (f)–(i) Comparison between the electric field profiles in 3D CR and 2D CR for selected wavelengths brought as examples of the frequency dependence [corresponding to the points in (e)]. These panels highlight the dispersive emission angle of 2D CR versus the nondispersive emission angle of 3D CR. θ [in (f) and (d)] and φ_1 and φ_2 [in (h) and (f)] are the angles between the electron trajectory and the direction of electromagnetic wave emission, $\vec{k}_{3D\text{CR}}$ and $\vec{k}_{2D\text{CR}}$, respectively.

conversion mechanism from electrical signal to plasmonic excitations [34,40]. Recent studies observed analogs of 2D CR in metasurfaces and other nanophotonic systems using an electromagnetic wave that replaced the emitting charged particle by a mathematical counterpart [41,42]. However, no experiment thus far has ever reported the observation of 2D CR by free electrons or by any charged particle. Therefore, none of the unique features emanating from the 2D nature of the emission has been observed.

Here, we present the first observation of 2D CR by free electrons. We use dispersion engineering of a metal-dielectric multilayered nanostructure to create 2D waves with phase velocities that match to the velocities of the electrons and, thus, fulfill the required extended phase matching. The 2D waves are the hybridization of an SPP (at the interface of Au-SiO₂) with a waveguide photonic mode (SiO₂-Si₃N₄-vacuum). The resulting dispersion satisfies extended phase matching over a wide range of electron kinetic energies (93–200 keV). This way, we achieve

record-high emission rates and the unique spectral features associated with 2D CR. We utilize this enhanced interaction to provide an experimental support for a recent paradigm shift, predicting the entanglement of the electrons with the wave they emit [43].

The radiation in every optical environment that is created by free or bound electrons, including *all* CR effects, can be conveyed in the language of *photonic quasiparticles* (PQPs) [44]. The emitted PQP can be either a photon in a 3D dielectric medium [13,14,17,18], a polariton in a 2D material [34,45,46], a surface plasmon polariton on an interface between materials [47,48], or a phonon polariton in a crystalline solid [49], etc. All these are forms of propagating PQPs, defined by a relatively long lifetime (longer than the cycle of the PQP) and long spatial extent (longer than the wavelength of the PQP). Their propagating nature enables them to satisfy extended phase matching with the emitting electron, thus becoming part of a Cherenkov-type process. Other types of PQPs such as bulk plasmons

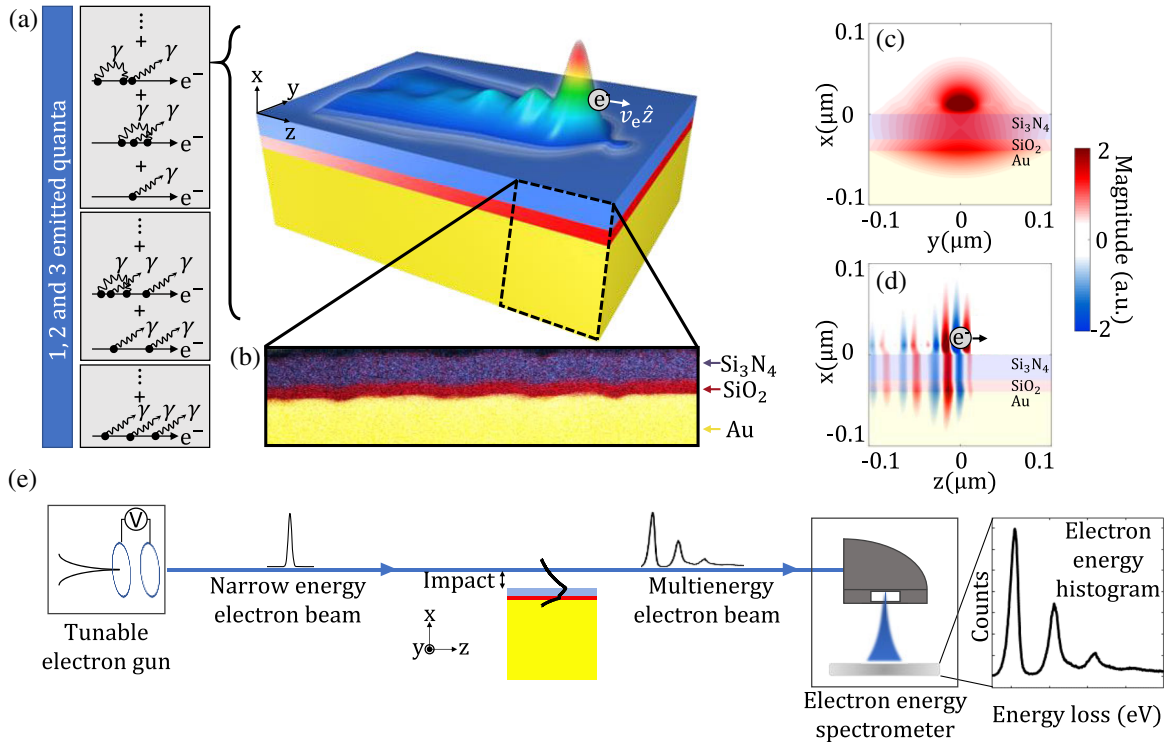


FIG. 2. The experimental setup for the 2D CR measurement. (a) Schematics of a free electron traveling above our metal-dielectric multilayer structure emitting 2D CR. The YZ cross section of the radiated electric field (z component) is presented, highlighting its copropagation with the electron. The schematic represents the emission of a single quanta of PQP (exemplified by the Feynman diagrams of one-photon emission), which is part of the joint electron-photon quantum state. Higher-order processes are also possible as shown in the other Feynman diagrams. (b) Cross-section image of the metal-dielectric multilayer structure. Layers are presented in different colors according to an energy-dispersive x-ray (EDX) spectroscopy measurement (see Appendix A). (c),(d) The field distribution of the PQP created by 2D CR through its XY (c) and XZ (d) cross sections. To maximize the overlap with the free electron, the sample is engineered to support a confined (c) PQP with a large field distribution in its evanescent tail that extends out of the structure (d). (e) Illustration of the experiment, wherein an electron beam propagates parallel to the sample surface and emits multiple quanta of PQPs. The emission events are imprinted on the electron energy spectrum as discretized energy loss events measured in the EELS. The inset shows a characteristic EELS measurement, featuring three 2D CR peaks beyond the zero-loss peak. The distance between the electron beam centroid to the sample surface is the impact parameter.

and surface plasmons [50–58] are nonpropagating (due to a below-cycle lifetime or spatial extent) and, thus, cannot take part in Cherenkov-type processes. Hereinafter, we focus on the *propagating* PQPs.

II. EXPERIMENTAL SETTINGS

Obtaining 2D CR requires a careful design of the PQP's dispersion such that it is phase matched with the moving electron over a distance of multiple wavelengths. We utilize a metal-dielectric multilayer structure [Au-SiO₂-Si₃N₄, Fig. 2(b)] supporting hybrid photonic-plasmonic modes [59,60] whose dispersion can be carefully tuned by the system's geometry [61,62]. Hence, we design such a structure [Figs. 2(a)–2(d)] to match the phase velocity of the PQPs to the electron velocity in a transmission electron microscope (TEM)—providing the ability to achieve the Cherenkov condition over a range of PQP energies (2.083–2.295 eV) and electron kinetic energies (93–200 keV). Another advantage of this structure is that, despite its PQPs being confined to the surface, they have much of their energy in the evanescent tail that is extended relatively far to the vacuum where the electrons are passing, leading to enhancement of the interaction efficiency [Figs. 2(c) and 2(d)].

Our experimental setup, shown in Fig. 2(e), includes a highly directional electron beam in grazing angle conditions, positioned at a distance (impact parameter) of tens of nanometers from the surface and sustained along tens to hundreds of microns (see Ref. [63] and Appendix A). This setup allows us to control several degrees of freedom that affect the 2D CR. By varying the electron kinetic energy, the energy of the emitted PQP is tuned, while varying the impact parameter and interaction length [Fig. 2(e)] affects the emission probability (the coupling strength) between the electron and the PQPs. These properties are then inferred from electron energy loss spectroscopy (EELS). Energy shifts as small as approximately 10 meV can be identified (see Appendix A).

III. RESULTS

Figure 3(a) presents the first EELS peak, showing that it redshifts for higher electron velocities, as expected from the CR extended phase-matching theory. This redshift has never appeared in previous EELS measurements, since all EELS experiments so far did not include extended phased-matched interactions. The EELS arising from interactions with nonpropagating PQPs is mostly independent of the electron velocity (though slighter blueshifts can occur for higher electron velocities due to a frequency dependence of the electron coupling strength to optical excitations).

In Fig. 3(b), we show how the 2D CR theory predicts the locations of the first EELS peak in every measurement. Each peak emission frequency can be approximately

determined by the intersection point of a line with slope equal to the electron velocity with the PQP dispersion (Fig. 6). This intersection explains the observed redshift of the emitted PQP with increasing electron energy. Had the electron interacted with only nonpropagating surface or bulk plasmons, as in previous EELS experiments that also show multiple emission events, e.g., Refs. [50–58,65,66], the EELS peaks would not have been altered as a function of the electron velocity, and the spectral redshift could not have been observed.

Apart from the specific spectral peak locations, the 2D CR theory (Supplemental Material, Note 1 [64]) also matches the spectral shape of the measured peak [Fig. 3(c)]. Notably, the asymmetric profile is a hallmark of 2D CR into lossy PQPs [34]. The excellent agreement between the theory and experiment enables us to more precisely determine the experimental parameters, since the spectral profile of 2D CR is highly sensitive to the impact parameter with a 10-nm accuracy.

IV. THE QUANTUM PHOTONIC NATURE OF 2D CR

The spontaneous emission process observed here as 2D CR provides insights on the quantum nature of free-electron radiation arising from the photonic description of the light itself. This contrasts with quantum effects arising from the wave nature of the electron that are revealed in stimulated emission and absorption processes, such as previously observed in inverse CR [63] and inverse-Smith–Purcell [67]. The quantum photonic nature of free-electron radiation has recently been under intense theoretical investigation [43,68–75]. The CR effect, like any other form of free-electron radiation, was surmised to be an emission process of classical light [9,43,73–75] (i.e., a Glauber coherent state in the quantum optics nomenclature). Recent theoretical advances [43,68–75] create a paradigm shift in the understanding of spontaneous emission from free electrons: Only an electron with a (coherently) wide energy uncertainty could emit classical light. An electron with energy uncertainty narrower than the energy of its emitted photons should become entangled with these photons [43,73–75].

Our results provide experimental evidence in support of this new paradigm, by having a narrow-enough electron energy uncertainty. Thus, each electron becomes in an entangled state with the PQPs it emits, which enables measuring the emission properties—both spectral shape and number of emission events—from the electron energy loss. This quantized nature is found in some of our EELS measurements, exhibiting multiple loss peaks with a separation of $\hbar\omega_0$, where ω_0 is the peak frequency of the PQP [Figs. 4(a) and 4(b)]. Each energy loss peak represents an emission of an integer number of PQPs. For comparison, for the electron to emit classical light (or

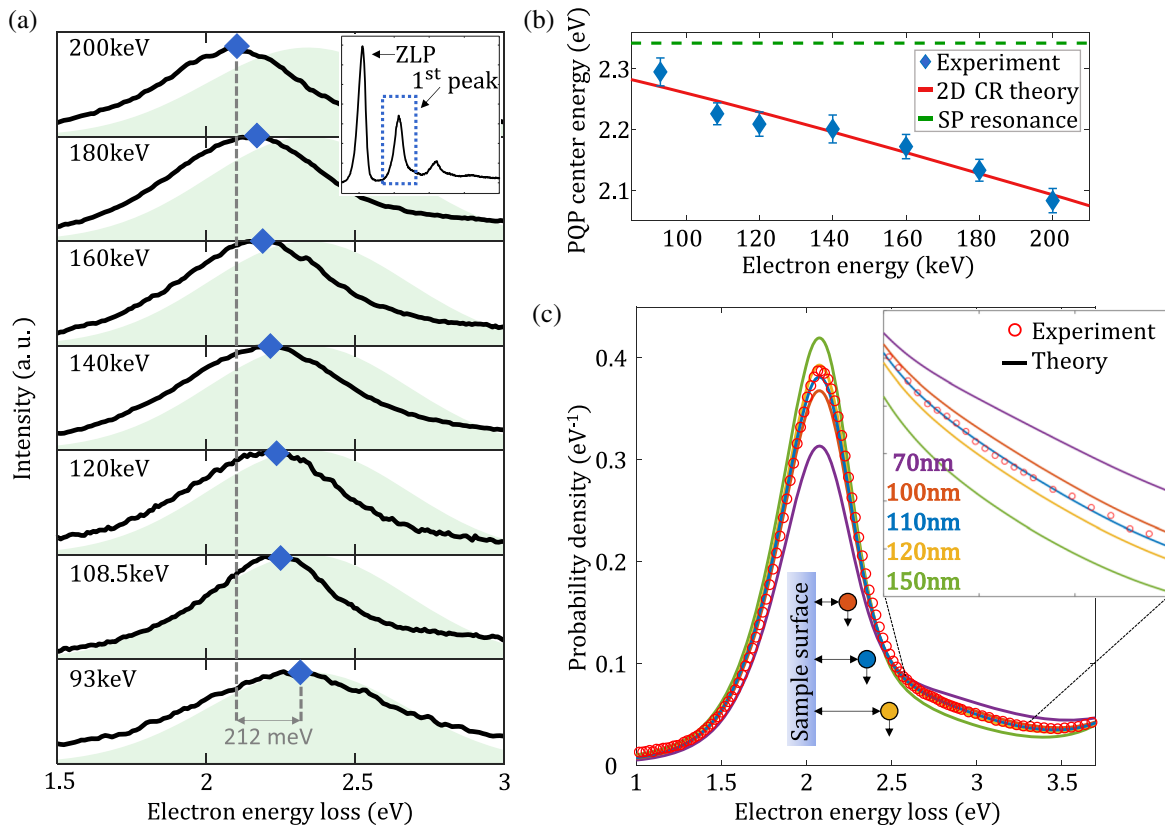


FIG. 3. First observation of 2D CR: satisfying the Cherenkov extended phase-matching condition. (a) The first EELS peak of each measurement (solid black line) for electrons grazing the multilayer structure. Increasing the electron energy results in a redshift of the peak, a signature of 2D CR. The shifting peak stands in contrast to EELS of common nonpropagating surface plasmon resonances, which remain constant when changing the electron energy (light green). The inset presents a characteristic raw measurement. (b) Comparison of experiment and theory. The measured peak energies from (a) (blue diamonds) are compared to theory of 2D CR into PQPs (red; see calculation in Supplemental Material, Note 1 [64]) and to the excitation of nonpropagating surface plasmon (SP) mode (dashed green line). Only the former shows agreement with our measurements. (c) Analysis of the EELS peak shape of 2D CR: comparison of theory and experiment. The first EELS peak is shown for a range of impact parameters, exhibiting the hallmark asymmetrical profile of the 2D CR emission spectrum, similar to Fig. 1(e). The spectrum has its peak at the Cherenkov threshold, a feature of 2D CR that differs substantially from the case of 3D CR. The good match of the simulated peak shape and location (colored solid lines) with the measured data (red circles) provides additional evidence for our observation of 2D CR and allows extraction of the effective impact parameter of the electron beam centroid with 10 nm accuracy. The inset shows an enlargement, which provides a more precise estimate of small changes in the impact parameter. The upward slope at the right edge of the spectrum arises from the second EELS peak.

classical 2D CR), its energy uncertainty must be wider, as shown in Fig. 4(c).

Figure 4(c) explains the transition from classical state to entangled state of the free-electron radiation when reducing the electron's energy uncertainty. The bottom row in Fig. 4(c) shows that the photonic density matrix of light emitted by an electron with a wide energy uncertainty can approach a Glauber coherent state, i.e., classical light. The emission of classical light further requires the electron temporal duration to be shorter than the emitted field cycle (which, given the wide energy uncertainty, is possible but not necessary). This condition is commonly occurring for radiation in the radio-frequency and microwave regimes, where the field cycle is long. However, this logic cannot be easily extended to the optical regime. Indeed, this condition is violated in our experiment, and, in fact, we expect it to be

similarly violated in almost all electron radiation experiments in the optical regime (and in higher frequencies such as x rays).

The measured EELS [Figs. 4(a) and 4(b)] closely resemble the top row in Fig. 4(c). There, the photonic density matrix of light contains near-zero off-diagonal terms, implying that the photons are in a nearly fully entangled state with the electron. Therefore, the EELS measurement provides indirect evidence showing that the CR process causes electrons to become in an entangled state with the PQPs they emit (as predicted very recently in Ref. [43]). It is important to note that the theory supporting our analysis is derived by a few recent studies that create a paradigm shift of how we understand the quantum nature of free-electron–photon interactions [43,73–75]. Our measurement is the first to provide

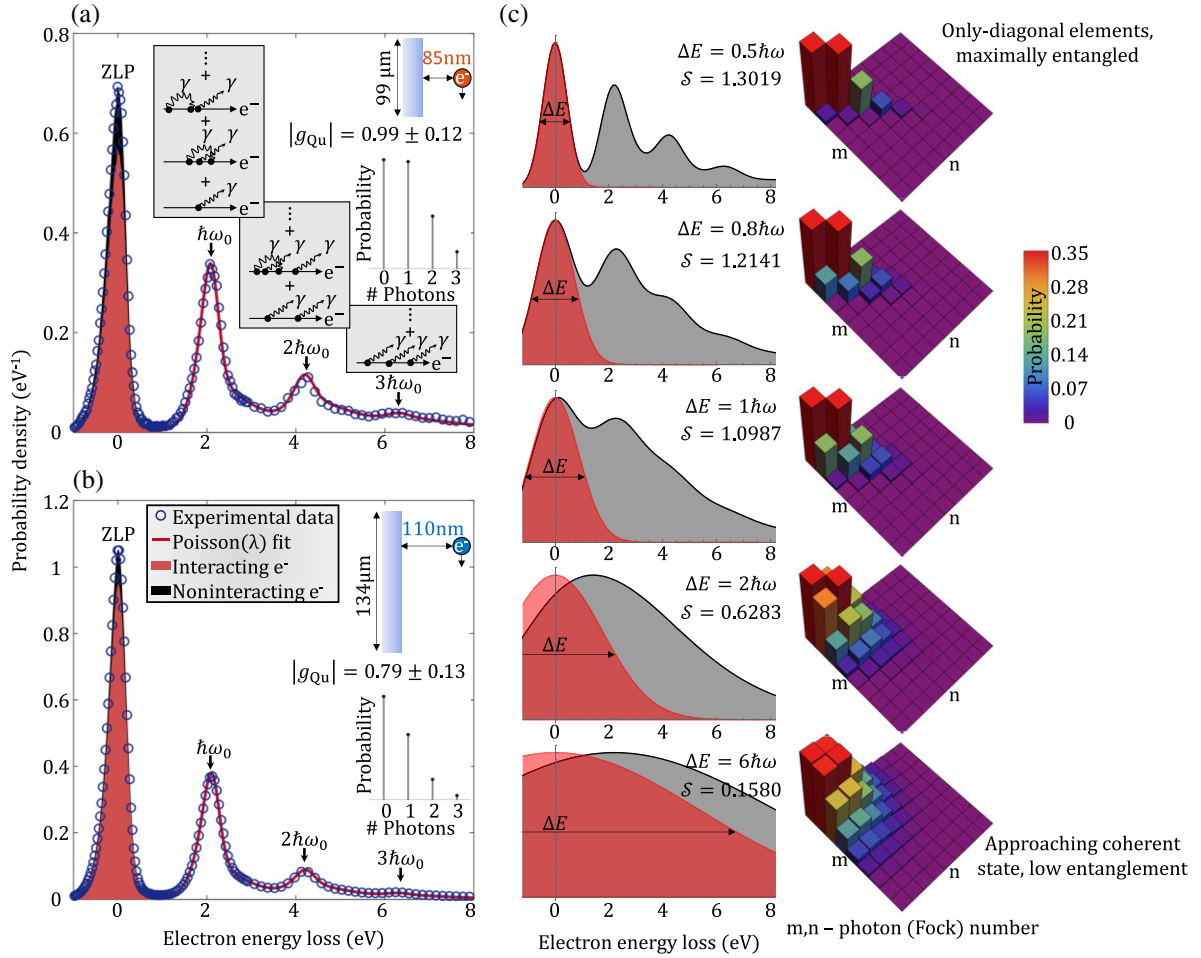


FIG. 4. Measurement of quantized radiation by free electrons: high-order emission of multiple photonic quasiparticles. (a),(b) EELS measurements of 200 keV electrons (blue circles) for two different impact parameters and effective interaction lengths reveal the quantized photonic nature of 2D CR by showing multiple peaks equally separated by the PQP energy. The suggested model [solid red curve, Eq. (2)] follows the recorded data precisely and allows the extraction of various parameters: (i) the total probability to emit zero, one, two, or three PQP (shown in the inset)—this probability follows a Poisson distribution according to the Feynman diagrams in (a) that include multiple emission and reabsorption events in each multiphoton emission process—(ii) a fairly substantial quantum coupling strength $|g_{\text{Qu}}| = \sqrt{\lambda}$ with λ being the Poisson distribution parameter; (iii) the ratio between the electrons that do and do not interact (red and black filling of the ZLP peak, respectively). No features are observed in the gain side of the spectra. (c) Theoretical analysis of the joint electron-PQP state, showing conditions for the emitted photons to be in an entangled state with the emitting electron and how they depend on the electron (coherent) energy uncertainty. EELS (left column) and the corresponding photonic density matrix in the Fock basis (for the peak frequency; right column) are simulated for different values of electron energy uncertainty using $|g_{\text{Qu}}|^2 = 1$, to resemble the case in (a). Each EELS is found by tracing out the photonic part of the joint density matrix, whereas each photonic density matrix is found by tracing out the electron part. The top row shows the case of an electron energy uncertainty narrower than the photon energy that creates a maximally entangled electron-PQP state. The bottom row shows the case of an electron energy uncertainty much wider than the photon energy, which can represent a short-duration electron pulse that creates a separable electron-PQP state with a Glauber coherent (classical) PQP state. See Supplemental Material [64] and Appendix A for additional details regarding the quantum description of the process, parameter extraction, and data analysis. To quantify the degree of entanglement between the electron and its emitted photons, the von Neuman entropy S is calculated theoretically [76] for each of the above cases. The maximal possible entropy for the case of $g_{\text{Qu}} = 1$ is 1.3048, and for $\Delta E = 0.5\hbar\omega$, we reach an entropy of 1.3019, which is a signature of the strong correlations between the electron and the photons—which are close to be in a maximally entangled state (see Supplemental Material, Note 3.3 [64], for further details).

indirect experimental evidence for this new understanding by using electron emission into propagating modes. Direct evidence for the underlying entanglement requires a coincidence measurement between the electron and photons.

V. THEORETICAL DESCRIPTION OF THE 2D CR QUANTUM PHOTONIC NATURE

The EELS measurements presented in Figs. 4(a) and 4(b) allow to resolve individual PQP emission events. Such

results cannot be reproduced by classical electromagnetism, since it ignores the photonic nature of light. Thus, to quantify the efficiency of PQP emission, we recall that each CR process can be described as spontaneous emission by an electron into photonic vacuum fluctuations that are phased matched with the electron [44,77]. The quantized nature of the PQP emission can be captured by a compact scattering matrix description [78] (see Supplemental Material, Note 7 [64], for its derivation):

$$\hat{S} \triangleq \exp[g_{\text{Qu}} b a^\dagger - g_{\text{Qu}}^* b^\dagger a], \quad (1)$$

where b (b^\dagger) is the electron energy ladder operator that decreases (increases) the electron energy by a discrete amount and a (a^\dagger) is the annihilation (creation) operator of a PQP; g_{Qu} is the quantum coupling strength, which is a dimensionless parameter proportional to $\sqrt{L_{\text{eff}}} e^{-|k_x| x_0}$, with x_0 being the impact parameter, L_{eff} the effective interaction length, and k_x the PQP (imaginary) wave vector in the x direction (further details in Supplemental Material, Note 5 [64]).

The quantum theory of free-electron interaction with photons [78–81] shown in Eq. (1) can be used to show that the PQP emission should follow Poisson statistics (Supplemental Material, Note 3 [64]). The Poisson distribution also appears in different ways in classical processes to reflect the mean distance (or time) between collision events. In our case, the Poisson parameter satisfies $\lambda = |g_{\text{Qu}}|^2$, representing the average amount of emitted PQP quanta and indicating the quantum interaction strength. Based on this theory, we construct a model to describe the distribution of energy loss in our system, combining the 2D CR spectral density with the Poisson statistics:

$$\begin{aligned} \frac{dP}{du} = & \underbrace{s \left(p \cdot \sum_{n=0}^{\infty} e^{-\lambda} \frac{\lambda^n}{n!} f_n(u) + (1-p)f_0(u) \right)}_{\text{Measured EEL signal}} \\ & + (1-s) \left(p \cdot \sum_{n=0}^{\infty} e^{-\lambda} \frac{\lambda^n}{n!} f_n(u) + (1-p)f_0(u) \right), \end{aligned} \quad (2)$$

where dP/du is the probability density that describes the EELS following all emission events as a function of the lost energy u . The probability density to emit n PQP quanta, $f_n(u)$, is constructed from the previous order by the recursive convolution $f_n(u) = f_{n-1}(u) * f_{\text{PQP}}(u)$, with $f_{\text{PQP}}(u)$ being the spectral density of the PQP (see Supplemental Material, Note 1 [64], for its derivation). $f_0(u)$ is the initial energy distribution of the electron beam, composed of coherent and incoherent contributions [also called the zero-loss peak (ZLP)], s is the probability to detect an electron in our setup, and p is the probability that an electron interacts with the sample

and, hence, is subjected to the Poisson process. This model involves two fitting parameters: (i) the Poisson parameter λ , which depends on the exact electron-photon interaction parameters (electron velocity, impact parameter, length of interaction); (ii) the product $s \cdot p$, which is related to the experimental settings and detection capabilities (detailed in Table S1 in Supplemental Material, Note 4 [64]). Equation (2) gives a good fit to the EELS measurements for the parameters obtained from our experiment [solid red line and blue dots in Figs. 4(a) and 4(b), respectively].

VI. EELS AS A METHOD TO QUANTIFY ELECTRON-PHOTON COUPLING STRENGTH

Figure 5 summarizes multiple EELS measurements with varying impact parameters and interaction lengths, showing the quantum coupling strength g_{Qu} in each case. The effective interaction length of each spectrum is extracted from fitting it to theory, showing a good agreement with the measured values of the maximal interaction length (see Supplemental Material, Note 5 [64]). The values of g_{Qu} range between 0.51 and 0.99, directly implying that higher-order processes, such as multiphoton emission, are not negligible in our CR experiment (Supplemental Material, Note 4 [64]). These g_{Qu} values are more than 2 orders of magnitude larger than in previous free-electron experiments [2,5,6,63,67,81–86] (see comparison in Supplemental Material, Note 6 [64]). Furthermore, these results are consistent with an *ab initio* model that uses macroscopic quantum electrodynamics [44,77] to calculate the coupling strength (see Supplemental Material, Note 3 [64]). This model also shows the qualitative scaling of g_{Qu} : linearly dependent on the square root of the interaction length and exponentially dependent on the impact parameter.

We emphasize that the quantum coupling strength g_{Qu} can be related to the coupling strength $g = g_{\text{Qu}} \sqrt{N}$ of stimulated free-electron processes, as in PINEM [3,4], where N is the number of photons stimulating the process. because of the large number of photons involved in stimulated processes (often relying on intense femto-second lasers), the stimulated g is much bigger and can quickly exceed unity. In contrast, it is rather hard to reach an intrinsic g_{Qu} of the order of unity.

VII. DISCUSSION: DOES THE ELECTRON BECOME ENTANGLED WITH A SINGLE- OR A MULTIMODE PHOTONIC STATE?

The theory in Eq. (1) considers a single-mode description of the PQP, despite its bandwidth that may call for a multimode quantum-optical theory. The good match with the experimental results shows that the single-mode theory is accurate for predicting the EELS amplitudes. A full analysis of the 2D CR effect should go beyond a

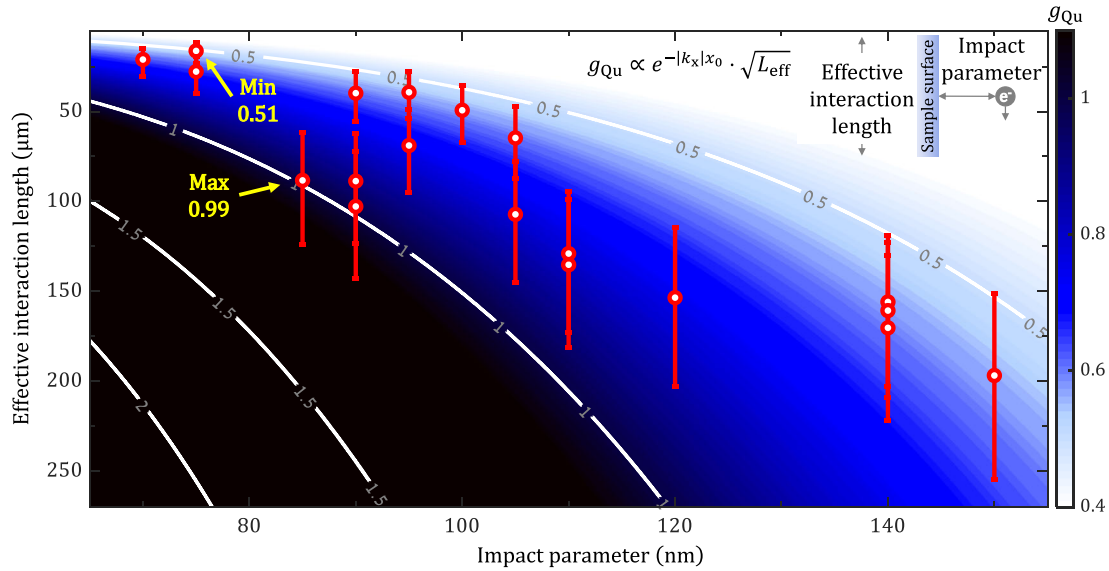


FIG. 5. Quantum coupling strength between free electrons and photonic quasiparticles. The quantum coupling strength is proportional to $g_{\text{Qu}} \propto e^{-|k_x|x_0} \cdot \sqrt{L_{\text{eff}}}$ and its values are extracted for 19 EELS measurements. Each value is overlaid on a theoretical calculation of the quantum coupling (colored background), derived in Supplemental Material, Notes 1 and 5 [64]. The calculated g_{Qu} is averaged over the electron beam Gaussian spatial distribution (with a standard deviation of 30 nm; see Supplemental Material, Note 5 [64], for more details). The red error bars represent a 10-nm difference in the impact parameter. The horizontal error bar for all data points is 10 nm in width, stemming from the fit resolution of the impact parameter [Fig. 3(c)]. All the measurements in this figure are with 200-keV electrons.

single-mode theory and consider the bandwidth of the emitted PQPs. Generally, the full quantum state of PQPs is composed of both (i) emission of multiple PQPs of different frequencies (e.g., $|1_{\text{PQP},\omega_1}, 1_{\text{PQP},\omega_2}, 1_{\text{PQP},\omega_3}\rangle$) and (ii) emission of Fock states of different orders (e.g., $|3_{\text{PQP},\omega}\rangle$).

As recently described in a theory paper [43], determining whether the emission is a mixed state or a pure state depends on the (coherent) energy uncertainty of the emitting electron. If the electron energy uncertainty is smaller than the PQP energy bandwidth, then the electron emits distinguishable PQP states with different frequencies within the PQP bandwidth [case (i) above]. Therefore, the resulting joint state contains entanglement between the electron and a multimode photonic state. In contrast, if the electron energy uncertainty is much wider than the PQP energy bandwidth, then the electron emits pure PQPs, each containing the entire PQP bandwidth [case (ii) above]. Therefore, the resulting joint state contains entanglement only between the electron and multiple PQP Fock states of different orders. The coherence of each PQP Fock state in the latter case can be understood from noting that the electron cannot distinguish between different modes within the PQP bandwidth. Consequently, only in this latter case may the PQP be rigorously considered as a single-mode photonic state.

To estimate the coherent energy uncertainty of the electron, we can rely on a recent study that measures it to be around 0.3 eV at full width at half maximum

(FWHM) for the same electron source that we use, although in a different TEM system [87,88]. The bandwidth of the PQP in our experiment is less than 0.2 eV at FWHM. This supports the single-mode treatment in Eq. (1). An additional consideration altering the resulting photonic state of the PQP is its limited coherence length, which in our case is approximately 2 μm due to optical losses. Since the coherence length is an order of magnitude shorter than the interaction length, the PQPs can be distinguished by their point of creation along the surface, creating a photonic state akin to case (i) instead of case (ii), but distinguishable in space rather than frequency. Drawing a certain conclusion about the precise quantum state of the multi-PQP emission requires a more advanced quantum-optical detection, such as a cathodoluminescence scheme that involves autocorrelation measurements.

Our analysis shows the prospects of EELS as a novel technique for measuring the quantum photonic state of free-electron radiation. As long as the electron energy uncertainty is narrower than the single-photon energy, such measurements contain indirect information on both the diagonal and the off-diagonal elements of the photonic density matrix, quantifying the entanglement in the joint electron-photon state. The idea that indirect measures can provide evidence of entanglement has been used before for other kinds of interactions (e.g., Refs. [89,90]). Such indirect measures for the quantum nature of the radiation can provide information beyond

conventional photon counter detectors (as often used for Cherenkov radiation). Indeed, photon counting would have failed to identify the difference between the photonic state in our system and a Glauber coherent state, because this difference lies outside the diagonal elements of the photonic density matrix [91] and is instead hidden in the off-diagonal elements [Fig. 4(c) right column]. Nevertheless, more work must be done to provide direct evidence of entanglement between the electron and the PQPs it emits. This, for example, could be done by coincidence measurement between the EELS and a cathodoluminescence detector capturing the emitted PQPs [92–94].

VIII. DISCUSSION: COMPARISON WITH OTHER MULTIPLE-PEAK EELS MEASUREMENTS

It is insightful to compare our measurements to previous EELS studies that observe multiple loss peaks [50–58]. In these studies, the loss peaks emanate during the electron penetration through the sample or reflection from it, exciting matter resonances linked with nonpropagating PQPs (e.g., bulk plasmons). In our case, the electron stays in vacuum and interacts only through the optical near field. In terms of electron-PQP entanglement, we can now infer in hindsight, in light of the recent theoretical advances [43,73–75] and our analysis here, that these previous experiments [50–58] also excite multiple PQPs which are in an entangled state with the electron. The major difference is that all previous studies create such states with nonpropagating PQPs, which are usually not considered as photons due to their short lifetime. In contrast, our work is the first to excite this behavior with propagating PQPs, which are often considered for their photonic nature since they may be coupled out of the sample [95].

Our findings critically depend on the photonic nature of propagating PQPs. In contrast to propagating PQPs, other matter excitations that are often measured with EELS [50–58,65,66], such as bulk and surface plasmons, cannot realize the Cherenkov effect, because they are lossy, cannot propagate in the material, and occur at a single-frequency resonance independent of the electron energy. The distinction between the propagating PQPs and the nonpropagating matter excitations can be extracted from the dielectric constants of the materials composing the structure in which they propagate. While nonpropagating matter excitations appear as a single-frequency resonance at which the dielectric constant is purely imaginary, the propagating PQPs are guided at the interface between materials for which the (real parts of the) dielectric constants are one positive and one negative over a range of frequencies. This is why it is possible to excite them over a range of frequencies and use them to realize phenomena such as CR.

We also compare our measurements to another family of EELS studies that measure multiple loss peaks (e.g., Ref. [12]). In such studies, multiple plasmonic modes can be simultaneously excited by an electron moving in vacuum close to nanophotonic structures such as metallic cones [65,66], triangles [96], and spheres [97,98]. These measurements differ from our work, as they describe the excitation of single-photon quanta in multiple modes rather than multiple-photon quanta in a single mode. In these studies, the total number of photons is (up to) one, and the joint electron photon state can be written as a sum of expressions such as $|E_0 - \hbar\omega_1\rangle_e \otimes |1_{\hbar\omega_1}\rangle_{\text{ph}} + |E_0 - \hbar\omega_2\rangle_e \otimes |1_{\hbar\omega_2}\rangle_{\text{ph}} + \dots$. In contrast to these studies, each electron in our experiment excites multiple quanta of the same photonic mode. Thus, the joint electron-photon state can be written as a sum of expressions such as $|E_0 - \hbar\omega_1\rangle_e \otimes |1_{\hbar\omega_1}\rangle_{\text{ph}} + |E_0 - 2\hbar\omega_1\rangle_e \otimes |2_{\hbar\omega_1}\rangle_{\text{ph}} + \dots$.

A signature of this difference is that the EELS peaks in these previous studies are not equally spaced (since the modes are not necessarily equally spaced), whereas, in our experiment, the EELS peaks are equally separated by the photon energy. The reason that these studies did not yet observe multiple quanta is the smaller dimension of the nanophotonic structures, typically comparable to or smaller than a single wavelength. Thus, the sizes are too small for the realization of an extended phase matching between the surface modes and the free electrons.

IX. DISCUSSION: A COMPARISON BETWEEN BOUND-ELECTRON AND FREE-ELECTRON INTERACTIONS WITH LIGHT

Equation (1) highlights a major difference between free-electron spontaneous emission and the spontaneous emission of bound electron systems like atoms, quantum dots, and molecules, etc. In the case of a weak coupling in atom-photon interaction, the rotating wave approximation (RWA) is commonly used to neglect energy-nonconserving terms. The RWA breaks in the case of ultrastrong coupling between the atom and the photon [99]. In contrast, the case of free-electron–photon interaction is fundamentally different—the scattering matrix in Eq. (1) is exact and does not rely on the RWA [78,80].

The difference arises from the nature of free electrons as opposed to bound electrons. Unlike an excited atom, each free electron is (i) not limited to specific energy transitions and (ii) not limited to the emission of a single photon. The former holds since the electron has a continuum of energy levels. The latter holds because the electron energy is much larger than the photon energy (i.e., light emission is a very small perturbation to the electron). Mathematically, the difference originates from the commutation relations of the creation and annihilation operators of the matter part: In the Jaynes-Cummings model, for example, those operators

are σ_+ and σ_- , which do not commute [100]. However, the ladder operators for a free electron, b^\dagger and b , do commute.

Therefore, in this work, despite reaching the single-electron–single-photon interaction regime, no nonconserving terms are involved in the interaction. Instead, we are able to reach such a strong interaction by maintaining an extended phase-matched interaction. In comparison, such an extended phase matching is not practical in atomic physics, because the velocity of atoms is usually too far below the phase velocity of light.

X. DISCUSSION: HISTORICAL CONTEXT FOR THE QUANTUM NATURE OF FREE-ELECTRON RADIATION

The history of research on the quantum nature of free-electron radiation, and particularly CR, goes back as far as 1940 [101–103]. Ginzburg [101] and Sokolov [102] were the first to describe CR using a quantum mechanical formalism—predicting changes that were considered negligible relative to the classical theory (given the experimental capabilities of that time). Recent theoretical papers show additional, non-negligible, corrections to the classical CR theory that arise from the quantum nature of the electron—its wave properties, its spin, or its quantized orbital angular momentum [11,68,70]. The effect of the electron wave function in CR was even observed recently, through an inverse-CR experiment [63], building on contemporary demonstrations of quantum wave-function-dependent features in *stimulated* processes of laser-electron interactions [2,81,104–109]. In contrast to the above-mentioned experiments, which expose the quantum nature of electrons, our observation is based on a *spontaneous* process, which exposes the quantum nature of photons.

For both spontaneous emission and stimulated emission, there are two necessary conditions for the quantum nature of photons to come into play. Only when both are satisfied the emitted photons and the emitting electron are in an entangled state. (i) The photonic state must be significantly modified, as can be quantified by the fidelity between the pre- and postinteraction photonic states. Stimulated interactions can usually be described classically, because the initial photonic state is a Glauber coherent state that usually does not significantly change by emission or absorption (i.e., high fidelity). In contrast, in spontaneous interactions (as in our experiment), the initial photonic state is vacuum, and, thus, emission of even just a single photon completely changes the photonic state (i.e., fidelity zero). (ii) The electron state must be significantly modified, which can also be quantified by the fidelity between the pre- and postinteraction electron states. The fidelity may be estimated by the overlap between electron wave functions, as in Fig. 4(c) (noting that the relative phase must be considered as well). In our experiment, the electron energy uncertainty is narrower than the energy of the PQP, and,

thus, the final electron becomes orthogonal (fidelity zero) to the initial electron. Since both conditions (i) and (ii) are satisfied in our experiment, the emitted PQPs are in an entangled state with the emitting electron.

More generally, our results in 2D CR suggest that analogous experiments should be able to reveal the inherent quantum features of other free-electron radiation phenomena. Such phenomena include transition radiation [18], Smith-Purcell radiation [110], 3D CR [13,14], and other types of CR into confined PQPs in different structures. To reach electron-photon coupling strengths even stronger than what we observe, it is worth recalling that CR phenomena should appear in a wide variety of structure geometries, such as slab waveguides and van der Waals materials [111], or even lower-dimensional structures, like slot waveguides [112] and metallic nanowires [59,113].

XI. CONCLUSION AND OUTLOOK

In conclusion, we observed experimentally the free-electron emission of PQPs via the mechanism of 2D CR, where the PQP dispersion relation caused the Cherenkov extended phase-matching condition to occur in different frequencies for different electron energies. The dimensionality and bandwidth of 2D CR allowed us to unveil the quantum photonic nature of the effect. Moreover, our experiment delivered the strongest free-electron–light interaction to date, over 2 orders of magnitude stronger than previous experiments. Such a strong coupling, together with the indirect evidence for electron-photon entanglement in our experiment, could have intriguing consequences: For example, free electrons can provide a new way to efficiently generate quantum light such as single-photon [114] and multiphoton [115] Fock states, by postselection on electrons with a certain energy loss [92–94]. Measurement of the electron after its light emission can also be used for quantum state tomography of light without measuring (and destroying) the light state [116]—also providing a heralding mechanism for the emission of quantum light. Free-electron–photon entanglement can also be used to improve the sensitivity of cathodoluminescence detection [75].

Utilizing efficient coupling of the PQPs to free-space photons could help realize the prospects of electrons for bright quantum emitters, in line with predictions made over the past decade [10,114]. To show that the emitter is indeed very bright, we note that the effective lifetime of the 2D CR process is a few hundred femtoseconds (considering the interaction lengths, electron velocities, and extracted Poisson parameters in our experiments). This lifetime is consistent with the measured values of classical 3D CR [28], but in a far smaller bandwidth. The combined short lifetime at a relatively narrow bandwidth makes the brightness of 2D CR especially attractive.

The fact that the microscopic properties of the nanostructure and its PQPs have such an influence on the

interaction with electrons passing nearby in vacuum opens intriguing possibilities for electron spectroscopy of condensed matter phenomena that are usually confined to electrons inside the material. These prospects are especially intriguing given that the probe electron passes at a distance of tens (and often hundreds) of nanometers from the surface, where effects that relate to internal electron correlations and many-body electron physics are usually negligible. The general idea is that any condensed matter phenomenon that alters the property of a PQP with a tail extending into vacuum can similarly be probed using a 2D Cherenkov-type interaction as demonstrated here. Such a probing method is limited by not having a direct interaction, as the electrons do not penetrate the material. Nevertheless, this approach can be attractive for sensitive quantum phases and long-range coherence and correlations in quantum materials, which are properties that are easily destroyed by a direct interaction with an energetic electron.

Looking forward, we envision the use of 2D CR and its inverse effect for integrated on-chip free-electron quantum emitters [8,9,114] and laser accelerators [6,7]. The interaction strength presented here is for the first time sufficient to allow single-electron–single-photon interactions, opening the door for free-electron cavity quantum electrodynamics [81,82]. This new interaction regime could enable the use of free electrons for quantum information applications [117,118] by entangling them with light [78], encoding them with qubit states [117], and utilizing them to entangle light in spatially separated cavities [119].

The first preliminary results of this study were presented in CLEO 2021 [120].

Data availability.—The data supporting the findings of this study are available from the corresponding author upon reasonable request.

ACKNOWLEDGMENTS

The authors thank Dr. Guy Ankonina for performing the evaporation process during sample preparation. With regard to the measurement of the layer widths, we thank Dr. Larisa Popilevsky, who prepared the TEM-lamella sample, and Dr. Galit Atiya, who acquired the EDX measurement. Samples were prepared at the Technion’s Micro & Nano Fabrication Unit and their characterization performed at the electron microscopy center (MIKA) in the Department of Materials Science and Engineering at the Technion. The work is supported by the Israel Science Foundation (ISF), Grant No. 3334/19, and the European Research Council (ERC) Starting Grant No. 851780-NanoEP. S. T. acknowledges support by the Adams Fellowship Program of the Israel Academy of Science and Humanities. H. H. was sponsored in part by Singapore Ministry of Education (No. MOE2018-T2-2-189 (S)) and A*Star AME Programmatic Funds (No. A18A7b0058). X. L. was sponsored in part by the National Natural Science Foundation of China (NSFC)

under Grant No. 62175212, the National Natural Science Fund for Excellent Young Scientists Fund Program (Overseas) of China, the Fundamental Research Funds for the Central Universities (2021FZZX001-19), and Zhejiang University Global Partnership Fund.

APPENDIX A: EXPERIMENTAL METHODS

1. Multilayer structure considerations

The principles that guide our sample design and yield the chosen multilayer structure are as follows.

- (i) The chosen structure supports only a single surface mode, whose dispersion can be engineered by the thickness of the dielectric layers. Thus, both the surface plasmon resonance of the structure and the effective dielectric permittivity of the surface mode can be controlled [61,62] to allow phase matching for a large range of free-electron energies, which are available in a transmission electron microscope (TEM). The dispersion of the mode is given below in Fig. 6.
- (ii) A significant part of the mode extends outside the sample to overlap with the free electron. Thus, a stronger free-electron light coupling is reached, compared to other systems with the same effective refractive index (i.e., regular waveguides). The spatial distribution of the mode is shown in Figs. 2(c) and 2(d).

Given the above, the design of the nanophotonic multilayer structure is key in enabling the extended phase-matching conditions that are necessary for our measurement. Thus, the dielectric layer widths are chosen to ensure that we are able to observe the Cherenkov emission into the propagating surface mode, over a wide energy range. The layer widths deviate slightly from the designed parameters, but these deviations are still within the tolerance that enables measuring the expected effect—see Appendix A 3 for layer width measurement.

2. Sample preparation

A Si wafer is diced into 1×1 mm squares and subsequently sputtered (AJA International Inc. ATC 2200) with multiple layers in the following order: 5 nm Ti (adhesion layer), 200 nm Au, 10 nm SiO_2 , and 30 nm Si_3N_4 . We choose those layer thicknesses such that the energy of 2D CR emission are in the range of approximately 2–2.3 eV, to facilitate characterization in a TEM. A square with an optical-grade surface is selected and then attached to a TEM sample holder with its diagonal parallel to the electron beam optical axis [see Fig. 2(e) and Supplemental Fig. S5].

3. Thickness measurement

Since the exact thickness of each layer greatly influences the PQP dispersion, the actual deposited film thicknesses are confirmed by cross-section imaging in another TEM

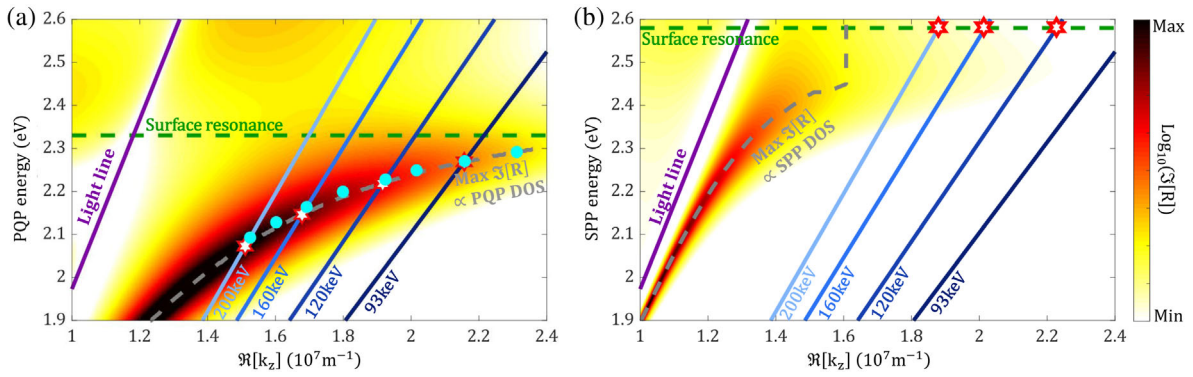


FIG. 6. Achieving Cherenkov phase matching for free electrons and optical excitations: comparison between the PQPs in our structure and the more conventional SPPs at the gold-vacuum interface. The colored backgrounds present the imaginary part of the reflection coefficient, which is proportional to the photonic density of states (DOS) of the surface modes, for (a) our metal-dielectric waveguide and (b) a gold-vacuum interface. The dashed gray curve follows the maximal value of the imaginary part of the reflection coefficient. The Cherenkov phase-matching condition is approximately given by the intersection (red stars) between the maximal DOS curve and a line with slope following the electron velocity (shades of blue). (a) The metal-dielectric waveguide structure: showing the velocity dependence of the energy at which the phase-matching condition is satisfied, corresponding to the shifts in the measured EELS peaks. The full calculation shows a slight blueshift compared with the predictions made by the DOS for most energies (i.e., the cyan dots are above the gray dashed line). The blueshift arises from including emission into all angles, which is considered in the full calculation and not captured by the density of state consideration. For large wave vectors, the PQPs are more lossy, leading to a slight redshift of the peak, which explains why for higher electron energies the full theory coincides more accurately with the PQP dispersion. (b) The gold-vacuum interface: showing that there are no intersection points with the curving dispersion of the gold-vacuum SPPs before it flattens to the constant surface plasmon resonance. Consequently, there is no velocity dependence and no shift in the EELS peaks.

(FEI Titan Themis G2). The lamella is prepared using a focused ion beam by a standard procedure (FEI Helios NanoLab DualBeam G3 UC). The layer thickness is measured to be 12.6 ± 1.2 nm for SiO_2 and 27.8 ± 1.1 nm for Si_3N_4 (average over 500×500 nm area). These numbers are used for the simulations in Fig. 3.

4. EELS

EELS measurements are carried out in a Jeol-2100 Plus TEM. The system is designed to also operate as an ultrafast TEM, driven by femtosecond laser pulses; however, the current experiments do not use lasers. The electron beam is created by thermal heating of a LaB_6 tip and is accelerated to the kinetic energies specified in the main text. Using converged beam electron diffraction (CBED) mode, we create parallel electron illumination with about 30 nm beam diameter and align it to graze the sample surface along a length of up to 250 μm . The sample stage translation is used to control the impact parameter (beam-sample distance) and the estimated maximal interaction length (maximal path over the sample by the beam).

EELS measurements are carried out using a Gatan GIF Quantum 965 spectrometer. Using low electron current, we configure the initial electron beam energy distribution (ZLP) to be as narrow as 0.4–0.6 eV in its FWHM. The spectrally narrow electron beam facilitates the observation of individual peaks in the energy loss spectrum. The ZLP shape is recorded far from the sample and is later used in the data analysis process (see Supplemental Material,

Note 4 [64]). After the ZLP measurement, the EELS from the grazing interaction with the sample is recorded. The detector dispersion is approximately 0.01 eV per channel for all measurements. The combination of a narrow ZLP with high spectrometer dispersion allows the capability of resolving the delicate shift in the 2D CR emission energy.

5. Data analysis

To determine the exact peak position in Figs. 3(a) and 3(b), we carry out the following procedure: We normalize the EELS measurements and subtract the ZLP from the EELS (this is a standard procedure that is, for example, also done in Ref. [81]). A single Gaussian function is matched to the first loss peak, and the mean of this Gaussian function is determined as the central frequency of the emitted PQP. To improve the sensitivity, we average the result over several independent measurements for each initial electron beam energy (this process is performed for each measurement separately). The final values in Fig. 3(c) are the averages over 2–12 repetitions of the same measurement in each energy. It is possible to resolve changes of the peak position with high accuracy (much better than the ZLP) due to the fact that the ZLP FWHM width is more than 4 times smaller than the PQP central energy (0.5 eV compared to approximately 2 eV), together with the high dispersion of our spectrometer.

We also provide in Fig. 3 the theoretical prediction as if the electrons in our experiment had interacted with the nonpropagating surface plasmon resonance of our

structure. The resonance frequency and width are determined using a full electromagnetic theory (Supplemental Material, Note 1 [64]) that captures the interaction of an electron with the plasmonic resonance (the nonpropagating PQP mode) without the interaction with the propagating PQP. This part of the energy loss spectrum does not depend on the electron energy, and, thus, we can simulate its Gaussian-style profile using electron energies under the Cherenkov threshold. We extract the specific height and width of the plasmon resonance EELS peak by simulating 30 keV electrons for the example in Figs. 3(a) and 3(b). The profile of the spectral shape [light green in Fig. 3(a)] is the result of a convolution with a 0.5 eV ZLP.

To extract the quantum coupling strength for each EELS measurement (as in Figs. 5 and 6), we carry out a nonlinear fitting process to find the correct theoretical description of those EELS curves. The full process is described in detail in Supplemental Material, Note 4 [64]. We carry out the same fit procedure for different impact parameters to produce Fig. 3(c).

APPENDIX B: PREDICTING THE PEAK FREQUENCY OF 2D CR

The most precise and rigorous way to obtain the spectrum of the 2D CR and its peak emission frequency is by using the full electromagnetic description of the interaction as given in Supplemental Material, Note 1 [64]. However, it is still worthy to describe a simpler theory that provides a more intuitive understanding of the extended phase-matching condition and determines the main trend of the peak emission frequency dependence on the electron velocity.

The Cherenkov extended phase-matching condition is mainly inferred from the intersection points on the dispersion diagram [Fig. 6(a)] between lines with slope equal to the electron energy and the curve of maximal imaginary part of the reflection coefficient, which is proportional to the density of states of the PQPs. These intersection points testify qualitatively on the experimental observation, because it predicts the redshift of the peak emission frequency when decreasing the electron energy.

This is not the full picture, though, since these intersection points reflect the extended phase-matching condition only between the electron and the PQP that is propagating parallel to it. Emission into PQPs that propagates in other angles can also satisfy the extended phase-matching condition and lead to a slight blueshift of the peak frequency relative to the one expected from the reflection coefficient calculation. The emission into these other angles becomes more dominant when losses are considered, leading to a broadening of the dispersion curve and, thus, to phase matching with additional modes. The full theory prediction is then back redshifted for large wave vectors due to the lossy nature of the PQP there. In the main text [Fig. 3(b)], we use the full 2D CR theory to compare with the experimental results.

APPENDIX C: COMPARISON TO THE CASE OF INTERACTION BETWEEN FREE ELECTRONS AND GOLD-VACUUM SURFACE PLASMONS

The main differences between our PQP modes and the gold-vacuum SPPs are as follows.

- (i) The SPP modes at a gold-vacuum interface can phase match with the TEM's free electrons only over a very limited electron energy range, which results in a small shift in the emission energy that is hard to observe with the resolution of our EELS. In contrast, the structure we design and measure supply phase matching over a wide electron energy range, thereby allowing us to observe the velocity-dependent shift of the emission with our EELS. This velocity dependence of the EELS peak is the most striking feature expected from Cherenkov-type effects, so it is important to us to design this specialized nanophotonic structure rather than use the simpler gold-vacuum interface.
- (ii) Losses limit the quality of the coupling between the electron and the SPP. In the gold-vacuum interface, losses severely limit SPP modes with larger effective refractive indices, becoming detrimental at indices around approximately 1.1, which is still below the requirement for phase matching in TEM energies. SPPs with larger effective refractive indices still exist, but their losses cause the coupling to electrons to become very broad, and then the dependence on electron velocity vanishes and the mode itself no longer propagates.

The comparison between the mode in our structure and the SPP mode at a gold-vacuum interface is given in Fig. 6.

APPENDIX D: IMPORTANT DIFFERENCES BETWEEN SPONTANEOUS AND STIMULATED FREE-ELECTRON RADIATION PHENOMENA

Our study investigates a spontaneous emission process by free electrons also known as Cherenkov radiation. This section shows the difference and the connection of the Cherenkov-type phenomenon to the complementary process of stimulated emission by free electrons, which has received a boost of interest in the past decade. A noteworthy example of a stimulated interaction is the experimental technique and theory of PINEM [2–4], which characterizes the electron after its interaction with an intense femtosecond laser pulse.

What may look like strong coupling in PINEM experiments is a completely different phenomenon than what we observe in our experiment. The difference arises from using an external laser pulse: The coupling strength of the PINEM interaction, usually denoted by g , benefits from the external stimulating field by a factor of \sqrt{N} (with N being the number of photons) scaling like $g = g_{\text{Qu}} \cdot \sqrt{N}$ (where g_{Qu} is the intrinsic quantum coupling strength discussed in this

manuscript). Then, of course, $g = g_{\text{Qu}} \cdot \sqrt{N}$ can quickly reach values much larger than unity. In contrast, it is much harder to reach a large quantum coupling strength, i.e., $g_{\text{Qu}} \sim 1$, without any external enhancement by \sqrt{N} . Our work is the first to reach the spontaneous strong coupling rather than the stimulated one.

Another important difference between the spontaneous process and the stimulated (PINEM) one is the origin of the quantization of the electron interaction spectrum. In PINEM, this quantization arises from the quantization of the electron itself (rather than the light), while the quantization of the electron energy spectrum in our case comes from the quantization of light rather than that of the electron. The model we use in our analysis of the experimental data is a result of recent advances in the exploration of free-electron quantum optics, going beyond the original theory of PINEM [78,80]. The resulting quantum-optical PINEM theory relies on the same scattering matrix of Eq. (1), where it was previously used to describe the interaction between free electrons and individual photons [78,80]. Our work here is the first to utilize this formalism to explain spontaneous processes, i.e., interactions between free electrons and the photonic quantum vacuum fluctuations.

-
- [1] J. H. Hubbell, *Review of Photon Interaction Cross Section Data in the Medical and Biological Context*, *Phys. Med. Biol.* **44**, R1 (1999).
- [2] B. Barwick, D. J. Flannigan, and A. H. Zewail, *Photon-Induced Near-Field Electron Microscopy*, *Nature (London)* **462**, 902 (2009).
- [3] F. J. García de Abajo, A. Asenjo-García, and M. Kociak, *Multiphoton Absorption and Emission by Interaction of Swift Electrons with Evanescent Light Fields*, *Nano Lett.* **10**, 1859 (2010).
- [4] S. T. Park, M. Lin, and A. H. Zewail, *Photon-Induced Near-Field Electron Microscopy (PINEM): Theoretical and Experimental*, *New J. Phys.* **12**, 123028 (2010).
- [5] J. Breuer and P. Hommelhoff, *Laser-Based Acceleration of Nonrelativistic Electrons at a Dielectric Structure*, *Phys. Rev. Lett.* **111**, 134803 (2013).
- [6] E. A. Peralta, K. Soong, R. J. England, E. R. Colby, Z. Wu, B. Montazeri, C. McGuinness, J. McNeur, K. J. Leedle, D. Walz, E. B. Sozer, B. Cowan, B. Schwartz, G. Travish, and R. L. Byer, *Demonstration of Electron Acceleration in a Laser-Driven Dielectric Microstructure*, *Nature (London)* **503**, 91 (2013).
- [7] N. V. Sapra, K. Y. Yang, D. Verduyck, K. J. Leedle, D. S. Black, R. Joel England, L. Su, R. Trivedi, Y. Miao, O. Solgaard, R. L. Byer, and J. Vučković, *On-Chip Integrated Laser-Driven Particle Accelerator*, *Science* **367**, 79 (2020).
- [8] G. Adamo, K. F. MacDonald, Y. H. Fu, C. M. Wang, D. P. Tsai, F. J. García de Abajo, and N. I. Zheludev, *Light Well: A Tunable Free-Electron Light Source on a Chip*, *Phys. Rev. Lett.* **103**, 113901 (2009).
- [9] F. J. García de Abajo, *Multiple Excitation of Confined Graphene Plasmons by Single Free Electrons*, *ACS Nano* **7**, 11409 (2013).
- [10] N. Talebi, *A Directional, Ultrafast and Integrated Few-Photon Source Utilizing the Interaction of Electron Beams and Plasmonic Nanoantennas*, *New J. Phys.* **16**, 053021 (2014).
- [11] N. Talebi, *Electron-Light Interactions beyond the Adiabatic Approximation: Recoil Engineering and Spectral Interferometry*, *Adv. Phys. X* **3**, 1499438 (2018).
- [12] A. Polman, M. Kociak, and F. J. García de Abajo, *Electron-Beam Spectroscopy for Nanophotonics*, *Nat. Mater.* **18**, 1158 (2019).
- [13] P. A. Cherenkov, *Visible Emission of Clean Liquids by Action of γ Radiation*, *Dokl. Akad. Nauk SSSR* **2**, 451 (1934).
- [14] I. E. Tamm and I. M. Frank, *Coherent In-Medium Fast-Electron Radiation*, *Dokl. Akad. Nauk SSSR* **14**, 109 (1937).
- [15] Z. Su, B. Xiong, Y. Xu, Z. Cai, J. Yin, R. Peng, and Y. Liu, *Manipulating Cherenkov Radiation and Smith–Purcell Radiation by Artificial Structures*, *Adv. Opt. Mater.* **7**, 1801666 (2019).
- [16] H. Hu, X. Lin, and Y. Luo, *Free-Electron Radiation Engineering via Structured Environments*, *Prog. Electromagn. Res.* **171**, 75 (2021).
- [17] C. Luo, M. Ibanescu, S. G. Johnson, and J. D. Joannopoulos, *Cherenkov Radiation in Photonic Crystals*, *Science* **299**, 368 (2003).
- [18] X. Lin, S. Easo, Y. Shen, H. Chen, B. Zhang, J. D. Joannopoulos, M. Soljačić, and I. Kaminer, *Controlling Cherenkov Angles with Resonance Transition Radiation*, *Nat. Phys.* **14**, 816 (2018).
- [19] F. Liu, L. Xiao, Y. Ye, M. Wang, K. Cui, X. Feng, W. Zhang, and Y. Huang, *Integrated Cherenkov Radiation Emitter Eliminating the Electron Velocity Threshold*, *Nat. Photonics* **11**, 289 (2017).
- [20] M. Voin and L. Schächter, *Enhanced Cherenkov-Wake Amplification by an Active Medium*, *Phys. Rev. Lett.* **112**, 054801 (2014).
- [21] J. Lu, T. Grzegorzczak, Y. Zhang, J. Pacheco, Jr., B.-I. Wu, J. Kong, and M. Chen, *Cherenkov Radiation in Materials with Negative Permittivity and Permeability*, *Opt. Express* **11**, 723 (2003).
- [22] S. Xi, H. Chen, T. Jiang, L. Ran, J. Huangfu, B. I. Wu, J. A. Kong, and M. Chen, *Experimental Verification of Reversed Cherenkov Radiation in Left-Handed Metamaterial*, *Phys. Rev. Lett.* **103**, 194801 (2009).
- [23] Z. Duan, X. Tang, Z. Wang, Y. Zhang, X. Chen, M. Chen, and Y. Gong, *Observation of the Reversed Cherenkov Radiation*, *Nat. Commun.* **8**, 14901 (2017).
- [24] M. Danos, S. Geschwind, H. Lashinsky, and A. van Trier, *Cherenkov Effect at Microwave Frequencies*, *Phys. Rev.* **92**, 828 (1953).
- [25] F. J. García de Abajo, A. Rivacoba, N. Zabala, and N. Yamamoto, *Boundary Effects in Cherenkov Radiation*, *Phys. Rev. B* **69**, 155420 (2004).
- [26] Z. W. Bell and L. A. Boatner, *Neutron Detection via the Cherenkov Effect*, *IEEE Trans. Nucl. Sci.* **57**, 3800 (2010).
- [27] Y. B. Xu and Z. Cheng, *Cherenkov Imaging: A New Modality for Molecular Imaging*, *Am. J. Nucl. Med.*

- Mol. Imag. **2**, 163 (2013), <https://www.ncbi.nlm.nih.gov/pmc/articles/PMC3477724/>.
- [28] A. K. Glaser, R. Zhang, J. M. Andreozzi, D. J. Gladstone, and B. W. Pogue, *Cherenkov Radiation Fluence Estimates in Tissue for Molecular Imaging and Therapy Applications*, *Phys. Med. Biol.* **60**, 6701 (2015).
- [29] T. M. Shaffer, E. C. Pratt, and J. Grimm, *Utilizing the Power of Cerenkov Light with Nanotechnology*, *Nat. Nanotechnol.* **12**, 106 (2017).
- [30] X. Lin, H. Hu, S. Easo, Y. Yang, Y. Shen, K. Yin, M. P. Blago, I. Kaminer, B. Zhang, H. Chen, J. Joannopoulos, M. Soljačić, and Y. Luo, *A Brewster Route to Cherenkov Detectors*, *Nat. Commun.* **12**, 5554 (2021).
- [31] A. Friedman, A. Gover, G. Kurizki, S. Ruschin, and A. Yariv, *Spontaneous and Stimulated Emission from Quasi-free Electrons*, *Rev. Mod. Phys.* **60**, 471 (1988).
- [32] L. Schachter, *Beam-Wave Interaction in Periodic and Quasi-Periodic Structures* (American Institute of Physics, New York, 1997), https://link.springer.com/book/10.1007/978-3-642-19848-9?utm_medium=referral&utm_source=google_books&utm_campaign=3_pier05_buy_print&utm_content=en_08082017.
- [33] F. J. García de Abajo, *Optical Excitations in Electron Microscopy*, *Rev. Mod. Phys.* **82**, 209 (2010).
- [34] I. Kaminer, Y. T. Katan, H. Buljan, Y. Shen, O. Ilic, J. J. Lopez, L. J. Wong, J. D. Joannopoulos, and M. Soljacic, *Efficient Plasmonic Emission by the Quantum Čerenkov Effect from Hot Carriers in Graphene*, *Nat. Commun.* **7**, ncomms11880 (2016).
- [35] H. Hu, X. Lin, L. J. Wong, Q. Yang, D. Liu, B. Zhang, and Y. Luo, *Surface Dyakonov–Cherenkov Radiation*, *ELight* **2**, 2 (2022).
- [36] O. Keller, *Electrodynamic Surface Dressing of a Moving Electron: Cherenkov-Landau Surface Shock Waves*, *Phys. Lett. A* **188**, 272 (1994).
- [37] O. Keller, *Local Fields in the Electrodynamics of Mesoscopic Media*, *Phys. Rep.* **268**, 85 (1996).
- [38] S. Liu, P. Zhang, W. Liu, S. Gong, R. Zhong, Y. Zhang, and M. Hu, *Surface Polariton Cherenkov Light Radiation Source*, *Phys. Rev. Lett.* **109**, 153902 (2012).
- [39] S. Liu, C. Zhang, M. Hu, X. Chen, P. Zhang, S. Gong, T. Zhao, and R. Zhong, *Coherent and Tunable Terahertz Radiation from Graphene Surface Plasmon Polaritons Excited by an Electron Beam*, *Appl. Phys. Lett.* **104**, 201104 (2014).
- [40] H. Hu, X. Lin, D. Liu, H. Chen, B. Zhang, and Y. Luo, *Broadband Enhancement of Cherenkov Radiation Using Dispersionless Plasmons*, *Adv. Sci.* **9**, 2200538 (2022).
- [41] P. Genevet, D. Wintz, A. Ambrosio, A. She, R. Blanchard, and F. Capasso, *Controlled Steering of Cherenkov Surface Plasmon Wakes with a One-Dimensional Metamaterial*, *Nat. Nanotechnol.* **10**, 804 (2015).
- [42] Y. Zhang, C. Hu, B. Lyu, H. Li, Z. Ying, L. Wang, A. Deng, X. Luo, Q. Gao, J. Chen, J. Du, P. Shen, K. Watanabe, T. Taniguchi, J. H. Kang, F. Wang, Y. Zhang, and Z. Shi, *Tunable Cherenkov Radiation of Phonon Polaritons in Silver Nanowire/Hexagonal Boron Nitride Heterostructures*, *Nano Lett.* **20**, 2770 (2020).
- [43] A. Karnieli, N. Rivera, A. Arie, and I. Kaminer, *The Coherence of Light Is Fundamentally Tied to the Quantum Coherence of the Emitting Particle*, *Sci. Adv.* **7**, eabf8096 (2021).
- [44] N. Rivera and I. Kaminer, *Light–Matter Interactions with Photonic Quasiparticles*, *Nat. Rev. Phys.* **2**, 538 (2020).
- [45] X. Shi, X. Lin, I. Kaminer, F. Gao, Z. Yang, J. D. Joannopoulos, M. Soljačić, and B. Zhang, *Superlight Inverse Doppler Effect*, *Nat. Phys.* **14**, 1001 (2018).
- [46] T. I. Andersen, B. L. Dwyer, J. D. Sanchez-Yamagishi, J. F. Rodriguez-Nieva, K. Agarwal, K. Watanabe, T. Taniguchi, E. A. Demler, P. Kim, H. Park, and M. D. Lukin, *Electron-Phonon Instability in Graphene Revealed by Global and Local Noise Probes*, *Science* **364**, 154 (2019).
- [47] H. Hu, D. Gao, X. Lin, S. Hou, B. Zhang, Q. J. Wang, and Y. Luo, *Directing Cherenkov Photons with Spatial Non-locality*, *Nanophotonics* **9**, 3435 (2020).
- [48] H. Hu, X. Lin, J. Zhang, D. Liu, P. Genevet, B. Zhang, and Y. Luo, *Nonlocality Induced Cherenkov Threshold*, *Laser Photonics Rev.* **14**, 2000149 (2020).
- [49] J. Tao, L. Wu, G. Zheng, and S. Yu, *Cherenkov Polaritonic Radiation in a Natural Hyperbolic Material*, *Carbon* **150**, 136 (2019).
- [50] R. H. Ritchie, *Plasma Losses by Fast Electrons in Thin Films*, *Phys. Rev.* **106**, 874 (1957).
- [51] H. Watanabe, *Experimental Evidence for the Collective Nature of the Characteristic Energy Loss of Electrons in Solids—Studies on the Dispersion Relation of Plasma Frequency*, *J. Phys. Soc. Jpn.* **11**, 112 (1956).
- [52] J. C. H. Spence and A. E. C. Spargo, *Observation of Double-Plasmon Excitation in Aluminum*, *Phys. Rev. Lett.* **26**, 895 (1971).
- [53] J. Schilling and H. Raether, *Energy Gain of Fast Electrons Interacting with Surface Plasmons*, *J. Phys. C* **6**, L358 (1973).
- [54] P. E. Batson and J. Silcox, *Experimental Energy-Loss Function, $\text{Im}[-1/\epsilon(q, \omega)]$, for Aluminum*, *Phys. Rev. B* **27**, 5224 (1983).
- [55] O. L. Krivanek, Y. Tanishiro, K. Takayanagi, and K. Yagi, *Electron Energy Loss Spectroscopy in Glancing Reflection from Bulk Crystals*, *Ultramicroscopy* **11**, 215 (1983).
- [56] P. Schattschneider, F. Fodermayr, and D.-S. Su, *Coherent Double-Plasmon Excitation in Aluminum*, *Phys. Rev. Lett.* **59**, 724 (1987).
- [57] S. L. Dudarev, L.-M. Peng, and M. J. Whelan, *Correlations in Space and Time and Dynamical Diffraction of High-Energy Electrons by Crystals*, *Phys. Rev. B* **48**, 13408 (1993).
- [58] R. F. Egerton, *Electron Energy-Loss Spectroscopy in the Electron Microscope* (Springer, New York, 2011), 10.1007/978-1-4419-9583-4.
- [59] R. F. Oulton, V. J. Sorger, D. A. Genov, D. F. P. Pile, and X. Zhang, *A Hybrid Plasmonic Waveguide for Subwavelength Confinement and Long-Range Propagation*, *Nat. Photonics* **2**, 496 (2008).
- [60] R. F. Oulton, V. J. Sorger, T. Zentgraf, R. M. Ma, C. Gladden, L. Dai, G. Bartal, and X. Zhang, *Plasmon Lasers at Deep Subwavelength Scale*, *Nature (London)* **461**, 629 (2009).
- [61] A. David, B. Gjonaj, Y. Blau, S. Dolev, and G. Bartal, *Nanoscale Shaping and Focusing of Visible Light in*

- Planar Metal–Oxide–Silicon Waveguides*, *Optica* **2**, 1045 (2015).
- [62] A. David, B. Gjonaj, and G. Bartal, *Two-Dimensional Optical Nanovortices at Visible Light*, *Phys. Rev. B* **93**, 121302 (2016).
- [63] R. Dahan, S. Nehemia, M. Shentcis, O. Reinhardt, Y. Adiv, X. Shi, O. Be, M. H. Lynch, Y. Kurman, K. Wang, and I. Kaminer, *Resonant Phase-Matching between a Light Wave and a Free-Electron Wavefunction*, *Nat. Phys.* **16**, 1123 (2020).
- [64] See Supplemental Material at <http://link.aps.org/supplemental/10.1103/PhysRevX.13.011002> for classical and quantum theoretical description of the 2D CR effect, experimental settings, and comparison to previous free-electron radiation experiments.
- [65] S. Guo, N. Talebi, W. Sigle, R. Vogelgesang, G. Richter, M. Esmann, S. F. Becker, C. Lienau, and P. A. Van Aken, *Reflection and Phase Matching in Plasmonic Gold Tapers*, *Nano Lett.* **16**, 6137 (2016).
- [66] N. Talebi, W. Sigle, R. Vogelgesang, M. Esmann, S. F. Becker, C. Lienau, and P. A. Van Aken, *Excitation of Mesoscopic Plasmonic Tapers by Relativistic Electrons: Phase Matching versus Eigenmode Resonances*, *ACS Nano* **9**, 7641 (2015).
- [67] Y. Adiv, K. Wang, R. Dahan, P. Broaddus, Y. Miao, D. Black, K. Leedle, R. L. Byer, O. Solgaard, R. J. England, and I. Kaminer, *Quantum Nature of Dielectric Laser Accelerators*, *Phys. Rev. X* **11**, 041042 (2021).
- [68] I. Kaminer, M. Mutzafi, A. Levy, G. Harari, H. H. Sheinfux, S. Skirlo, J. Nemirovsky, J. D. Joannopoulos, M. Segev, and M. Soljacic, *Quantum Čerenkov Radiation: Spectral Cutoffs and the Role of Spin and Orbital Angular Momentum*, *Phys. Rev. X* **6**, 011006 (2016).
- [69] S. Tsesses, G. Bartal, and I. Kaminer, *Light Generation via Quantum Interaction of Electrons with Periodic Nanostructures*, *Phys. Rev. A* **95**, 013832 (2017).
- [70] N. Talebi, *Interaction of Electron Beams with Optical Nanostructures and Metamaterials: From Coherent Photon Sources towards Shaping the Wave Function*, *J. Opt.* **19**, 103001 (2017).
- [71] A. Gover, R. Ianculescu, A. Friedman, C. Emma, N. Sudar, P. Musumeci, and C. Pellegrini, *Superradiant and Stimulated-Superradiant Emission of Bunched Electron Beams*, *Rev. Mod. Phys.* **91**, 035003 (2019).
- [72] A. Feist, S. V. Yalunin, S. Schafer, and C. Ropers, *High-Purity Free-Electron Momentum States Prepared by Three-Dimensional Optical Phase Modulation*, *Phys. Rev. Res.* **2**, 043227 (2020).
- [73] V. Di Giulio, O. Kfir, C. Ropers, and F. J. García de Abajo, *Modulation of Cathodoluminescence Emission by Interference with External Light*, *ACS Nano* **15**, 7290 (2021).
- [74] F. J. García de Abajo and V. Di Giulio, *Optical Excitations with Electron Beams: Challenges and Opportunities*, *ACS Photonics* **8**, 945 (2021).
- [75] O. Kfir, V. Di Giulio, F. Javier García de Abajo, and C. Ropers, *Optical Coherence Transfer Mediated by Free Electrons*, *Sci. Adv.* **7**, eabf6380 (2021).
- [76] V. Vedral, M. B. Plenio, M. A. Rippin, and P. L. Knight, *Quantifying Entanglement*, *Phys. Rev. Lett.* **78**, 2275 (1997).
- [77] S. Scheel and S. Buhmann, *Macroscopic Quantum Electrodynamics—Concepts and Applications*, *Acta Phys. Slovaca* **58**, 675 (2008), <http://www.physics.sk/aps/pub.php?y=2008&pub=aps-08-05>.
- [78] O. Kfir, *Entanglements of Electrons and Cavity-Photons in the Strong Coupling Regime*, *Phys. Rev. Lett.* **123**, 103602 (2019).
- [79] Y. Pan and A. Gover, *Spontaneous and Stimulated Emissions of a Preformed Quantum Free-Electron Wave Function*, *Phys. Rev. A* **99**, 052107 (2019).
- [80] V. Di Giulio, M. Kociak, and F. J. G. de Abajo, *Probing Quantum Optical Excitations with Fast Electrons*, *Optica* **6**, 1524 (2019).
- [81] K. Wang, R. Dahan, M. Shentcis, Y. Kauffmann, A. Ben Hayun, O. Reinhardt, S. Tsesses, and I. Kaminer, *Coherent Interaction between Free Electrons and a Photonic Cavity*, *Nature (London)* **582**, 50 (2020).
- [82] O. Kfir, H. Lourenço-Martins, G. Storeck, M. Siviş, T. R. Harvey, T. J. Kippenberg, A. Feist, and C. Ropers, *Controlling Free Electrons with Optical Whispering-Gallery Modes*, *Nature (London)* **582**, 46 (2020).
- [83] K. J. Leedle, R. F. Pease, R. L. Byer, and J. S. Harris, *Laser Acceleration and Deflection of 96.3 keV Electrons with a Silicon Dielectric Structure*, *Optica* **2**, 158 (2015).
- [84] K. J. Leedle, A. Ceballos, H. Deng, O. Solgaard, R. Fabian Pease, R. L. Byer, and J. S. Harris, *Dielectric Laser Acceleration of Sub-100 KeV Electrons with Silicon Dual-Pillar Grating Structures*, *Opt. Lett.* **40**, 4344 (2015).
- [85] D. Cesar, S. Custodio, J. Maxson, P. Musumeci, X. Shen, E. Threlkeld, R. J. England, A. Hanuka, I. V. Makasyuk, E. A. Peralta, K. P. Wootton, and Z. Wu, *High-Field Nonlinear Optical Response and Phase Control in a Dielectric Laser Accelerator*, *Commun. Phys.* **1**, 46 (2018).
- [86] P. Yousefi, N. Schönenberger, J. Mcneur, M. Kozák, U. Niedermayer, and P. Hommelhoff, *Dielectric Laser Electron Acceleration in a Dual Pillar Grating with a Distributed Bragg Reflector*, *Opt. Lett.* **44**, 1520 (2019).
- [87] F. Hasselbach, *Progress in Electron- and Ion-Interferometry*, *Rep. Prog. Phys.* **73**, 016101 (2010).
- [88] M. Tsarev, A. Ryabov, and P. Baum, *Measurement of Temporal Coherence of Free Electrons by Time-Domain Electron Interferometry*, *Phys. Rev. Lett.* **127**, 165501 (2021).
- [89] G. Nogues, A. Rauschenbeutel, S. Osnaghi, M. Brune, J. M. Raimond, and S. Haroche, *Seeing a Single Photon without Destroying It*, *Nature (London)* **400**, 239 (1999).
- [90] R. Dahan, A. Gorlach, U. Haeusler, A. Karnieli, O. Eyal, P. Yousefi, M. Segev, A. Arie, G. Eisenstein, P. Hommelhoff, and I. Kaminer, *Imprinting the Quantum Statistics of Photons on Free Electrons*, *Science* **373**, eabj7128 (2021).
- [91] J. H. Shapiro, G. Saplakoglu, S.-T. Ho, P. Kumar, B. E. A. Saleh, and M. C. Teich, *Theory of Light Detection in the Presence of Feedback*, *J. Opt. Soc. Am. B* **4**, 1604 (1987).
- [92] D. Jannis, K. Müller-Caspary, A. Béch e, A. Oelsner, and J. Verbeeck, *Spectroscopic Coincidence Experiments in Transmission Electron Microscopy*, *Appl. Phys. Lett.* **114**, 143101 (2019).

- [93] A. Feist, G. Huang, G. Arend, Y. Yang, J. Henke, A. S. Raja, F. J. Kappert, R. N. Wang, Z. Qiu, J. Liu, O. Kfir, T. J. Kippenberg, and C. Ropers, *Cavity-Mediated Electron-Photon Pairs*, *Science* **377**, 777 (2022).
- [94] N. Varkentina, Y. Auad, S. Y. Woo, A. Zobelli, J.-D. Blazit, X. Li, M. Tencé, K. Watanabe, T. Taniguchi, O. Stéphan, M. Kociak, and L. H. G. Tizei, *Cathodoluminescence Excitation Spectroscopy: Nanoscale Imaging of Excitation Pathways*, *Sci. Adv.* **8**, eabq4947 (2022).
- [95] B. Rothenhausler and W. Knoll, *Surface-Plasmon Microscopy*, *Nature (London)* **332**, 615 (1988).
- [96] J. Nelayah, M. Kociak, O. Stéphan, F. J. G. De Abajo, M. Tencé, L. Henrard, D. Taverna, I. Pastoriza-Santos, L. M. Liz-Marzán, and C. Colliex, *Mapping Surface Plasmons on a Single Metallic Nanoparticle*, *Nat. Phys.* **3**, 348 (2007).
- [97] M. W. Chu, C. H. Chen, F. J. García De Abajo, J. P. Deng, and C. Y. Mou, *Surface Exciton Polaritons in Individual Au Nanoparticles in the Far-Ultraviolet Spectral Regime*, *Phys. Rev. B* **77**, 245402 (2008).
- [98] M. W. Chu, V. Myroshnychenko, C. H. Chen, J. P. Deng, C. Y. Niou, and F. J. G. De Abajo, *Probing Bright and Dark Surface-Plasmon Modes in Individual and Coupled Noble Metal Nanoparticles Using an Electron Beam*, *Nano Lett.* **9**, 399 (2009).
- [99] A. Frisk Kockum, A. Miranowicz, S. De Liberato, S. Savasta, and F. Nori, *Ultrastrong Coupling between Light and Matter*, *Nat. Rev. Phys.* **1**, 19 (2019).
- [100] E. T. Jaynes and F. W. Cummings, *Comparison of Quantum and Semiclassical Radiation Theories with Application to the Beam Maser*, *Proc. IEEE* **51**, 89 (1963).
- [101] V. L. Ginzburg, *Quantum Theory of Radiation of Electron Uniformly Moving in Medium*, *Zh. Eksp. Teor. Fiz.* **10**, 589 (1940).
- [102] A. Sokolow, *Quantum Theory of Cherenkov Effect*, *Dokl. Akad. Nauk SSSR* **28**, 415 (1940).
- [103] R. T. Cox, *Momentum and Energy of Photon and Electron in the Čerenkov Radiation*, *Phys. Rev.* **66**, 106 (1944).
- [104] L. Piazza, T. T. A. Lummen, E. Quiñonez, Y. Murooka, B. W. Reed, B. Barwick, and F. Carbone, *Simultaneous Observation of the Quantization and the Interference Pattern of a Plasmonic Near-Field*, *Nat. Commun.* **6**, 6407 (2015).
- [105] A. Feist, K. E. Echternkamp, J. Schauss, S. V. Yalunin, S. Schäfer, and C. Ropers, *Quantum Coherent Optical Phase Modulation in an Ultrafast Transmission Electron Microscope*, *Nature (London)* **521**, 200 (2015).
- [106] K. E. Echternkamp, A. Feist, S. Schäfer, and C. Ropers, *Ramsey-Type Phase Control of Free-Electron Beams*, *Nat. Phys.* **12**, 1000 (2016).
- [107] G. M. Vanacore, I. Madan, G. Berruto, K. Wang, E. Pomarico, R. J. Lamb, D. McGrouther, I. Kaminer, B. Barwick, F. J. García de Abajo, and F. Carbone, *Attosecond Coherent Control of Free-Electron Wave Functions Using Semi-Infinite Light Fields*, *Nat. Commun.* **9**, 2694 (2018).
- [108] Y. Morimoto and P. Baum, *Diffraction and Microscopy with Attosecond Electron Pulse Trains*, *Nat. Phys.* **14**, 252 (2018).
- [109] G. M. Vanacore, G. Berruto, I. Madan, E. Pomarico, P. Biagioni, R. J. Lamb, D. McGrouther, O. Reinhardt, I. Kaminer, B. Barwick, H. Larocque, V. Grillo, E. Karimi, F. J. García de Abajo, and F. Carbone, *Ultrafast Generation and Control of an Electron Vortex Beam via Chiral Plasmonic near Fields*, *Nat. Mater.* **18**, 573 (2019).
- [110] S. J. Smith and E. M. Purcell, *Visible Light from Localized Surface Charges Moving across a Grating*, *Phys. Rev.* **92**, 1069 (1953).
- [111] D. N. Basov, M. M. Fogler, and F. J. F. Javier de Abajo, *Polaritons in van Der Waals Materials*, *Science* **354**, aag1992 (2016).
- [112] V. R. Almeida, Q. Xu, C. A. Barrios, and M. Lipson, *Guiding and Confining Light in Void Nanostructure*, *Opt. Lett.* **29**, 1209 (2004).
- [113] D. E. Fernandes, S. I. Maslovski, and M. G. Silveirinha, *Cherenkov Emission in a Nanowire Material*, *Phys. Rev. B* **85**, 155107 (2012).
- [114] X. Bendana, A. Polman, and F. J. García de Abajo, *Single-Photon Generation by Electron Beams*, *Nano Lett.* **11**, 5099 (2011).
- [115] A. Ben Hayun, O. Reinhardt, J. Nemirovsky, A. Karnieli, N. Rivera, and I. Kaminer, *Shaping Quantum Photonic States Using Free Electrons*, *Sci. Adv.* **7**, eabe4270 (2021).
- [116] A. Gorlach, A. Karnieli, R. Dahan, E. Cohen, A. Pe'er, and I. Kaminer, *Ultrafast Non-Destructive Measurement of the Quantum State of Light Using Free Electrons*, *arXiv:2012.12069*.
- [117] O. Reinhardt, C. Mechel, M. Lynch, and I. Kaminer, *Free-Electron Qubits*, *Ann. Phys. (N.Y.)* **533**, 2000254 (2021).
- [118] C. Mechel, Y. Kurman, A. Karnieli, N. Rivera, A. Arie, and I. Kaminer, *Quantum Correlations in Electron Microscopy*, *Optica* **8**, 70 (2021).
- [119] G. Baranes, R. Ruimy, A. Gorlach, and I. Kaminer, *Free Electrons Can Induce Entanglement between Photons*, *npj Quantum Inf.* **8**, 32 (2022).
- [120] Y. Adiv, H. Hu, S. Tsesses, R. Dahan, K. Wang, Y. Kurman, H. Chen, X. Lin, G. Bartal, and I. Kaminer, *Observation of 2D Cherenkov Radiation and Its Quantized Photonic Nature Using Free-Electrons*, in *Proceedings of the Conference on Lasers and Electro-Optics* (Optical Society of America, Washington, DC, 2021), p. FM1L.6, https://opg.optica.org/abstract.cfm?uri=cleo_qels-2021-FM1L.6&origin=search.